ELSEVIER

Surface Science 410 (1998) 351–361

surface science

Optical second-harmonic investigations of the isothermal desorption of SiO from the Si(100) and Si(111) surfaces

M.B. Raschke *, P. Bratu [1], U. Höfer

Max-Planck-Institut für Quantenoptik, D-85740 Garching, Germany
Physik Department, Technische Universität München, D-85747 Garching, Germany

Received 2 February 1998; accepted for publication 11 May 1998

Abstract

The isothermal desorption of SiO from the Si(100) and Si(111) surfaces was investigated by means of optical second-harmonic generation (SHG). Due to the high adsorbate sensitivity of this method, desorption rates could be measured over a wide range from 10^{-1} to 10^{-6} ML s^{-1}. From their temperature dependence between 780 and 1000 K, activation energies of $E_A = 3.4 \pm 0.2$ eV and $E_A = 4.0 \pm 0.3$ eV and pre-exponential factors of $n_0 = 10^{16 \pm 1}$ s^{-1} and $n_0 = 10^{20 \pm 1}$ s^{-1} for SiO desorption were obtained for Si(100) and Si(111), respectively. In the case of the Si(100) surface, a pronounced decrease of the first-order rate constants was observed upon increasing the initial coverage from 0.02 to 0.6 ML. The results are interpreted in terms of coverage-dependent oxygen-binding configurations, which influence the stability of the oxide layer. © 1998 Elsevier Science B.V. All rights reserved.

Keywords: Desorption; Oxygen; Second-harmonic generation; Silicon

1. Introduction

The growth of high-quality SiO_2 films by thermal oxidation of silicon requires substrate temperatures in excess of 900 K to facilitate O_2 diffusion through the oxide layer [1,2]. In the initial stages of this process, where O_2 directly impinges on to the silicon surface, oxidation competes with etching because of the formation of volatile SiO at these temperatures ([3] and references therein). For a detailed atomistic description of this complicated process, the determination of the structure of thin oxide layers and the identification of the reaction centers with the scanning tunneling microscope (STM) provide invaluable information [4–6], but also, the kinetic parameters of the reaction steps are of great interest. For their determination, a purely optical technique like second-harmonic generation (SHG) is particularly useful.

SHG is a sensitive in-situ monitor of the adsorbate coverage of silicon surfaces that is applicable at any surface temperature or gas pressure [7]. In the case of oxygen adsorption on Si(111), the sensitivity of this technique has been demonstrated in several previous experiments [8–14]. Recently, Shklyaev and Suzuki applied SHG rather successfully near the critical oxidation conditions [11,12]. For temperatures above 880 K, the oxide growth was shown to be strongly dependent on oxygen pressure. The subsequent decomposition was found to depend not only on the total oxide

* Corresponding author. Fax: +49 89 32905 200;
e-mail: raschke@mp9.mpg.de
[1] Present address: Siemens Microelectronics Center, Königsbrücker Str. 180, D-01099 Dresden, Germany.

0039-6028/98/$19.00 © 1998 Elsevier Science B.V. All rights reserved.
PII: S0039-6028(98)00389-6

coverage and surface temperature but also on the conditions of oxide growth.

The SHG experiments presented in this paper address just one of the relevant elementary steps of oxygen interaction with silicon surfaces, SiO desorption. We investigated the coverage and temperature dependence of this process in detail by performing isothermal measurements for both the Si(100) and Si(111) surfaces. In order to obtain quantitative results over a wide range of coverages, one emphasis has been on the careful calibration of the SHG response with temperature-programmed desorption (TPD). As a result of the high sensitivity of SHG to the number of Si-dangling bonds, initial oxygen coverages as low as 0.02 monolayer (ML) and desorption rates as low as 10^{-6} ML s^{-1} became experimentally accessible. The coverage dependence of the desorption rates suggests that even such thin adlayers decompose inhomogeneously. The deduced activation energy for desorption is similar for both surfaces. Combined with the results of previous investigations by Engel, Yu and others [15–22] using molecular-beam scattering and thermal desorption techniques, the SiO desorption from silicon is shown to obey an Arrhenius law over nearly 11 orders of magnitude. This leads to the conclusion that desorption is a direct process. However, the details of the kinetics depend on the morphology of the oxide layer.

2. Experimental

2.1. Experimental setup

The experiments were carried out in an ultrahigh vacuum system with a working pressure of $\sim 4\times10^{-11}$ mbar. The Si(100) and Si(111) samples, oriented to within 1/4°, were cut from 10-$\Omega\cdot$cm n-type wafers and mounted on a liquid-nitrogen-cooled sample holder. A NiCr/NiAl-thermocouple cemented on the backside of the samples and an infra-red pyrometer were used to measure the temperature with an absolute accuracy of ±10 K. For the cleaning procedure and desorption experiments, the sample temperature was controlled via direct resistive heating. Cleanliness and surface order were checked using Auger electron spectroscopy (AES) and low-energy electron diffraction (LEED). In order to prepare the adsorbate layers, the samples were exposed to research grade 99.998 vol.% molecular oxygen at pressures of $\sim10^{-7}$ mbar. A capillary array doser in front of the surface was employed for the Si(111) measurements; simple background dosing was applied in case of the Si(100) samples. In the temperature-programmed desorption (TPD) experiments, the desorbing SiO was detected using a quadrupole mass spectrometer (QMS) with a "Feulner cap" around the ionizer [23]. For optimal sensitivity, the whole assembly was mounted on to a translational stage and could be placed in front of the sample in a very reproducible way.

For the SHG measurements, 1064 nm pump radiation incident at 45° with respect to the surface normal was provided by Q-switched Nd:YAG lasers (Coherent Infinity with a pulse duration of 3.5 ns operating at a repetition rate of 30 Hz and Lumonics HY 400 with a pulse duration of 8 ns and a repetition rate of 10 Hz). It was verified that the employed laser fluence of 100 mJ cm^{-2} did not influence the measured desorption rate and that it was well below the damage threshold of the samples. In the case of Si(111)7×7, the polarizations of the incident pump radiation and detected SH light were chosen such that only the anisotropic component $\chi^{(2)}_{s,\xi\xi\xi}$ of the non-linear susceptibility tensor contributed to the measured second-harmonic signal [24]. For Si(100)2×1, the polarization of the pump beam was chosen to maximize the SH output.

2.2. Calibration of SHG response

The changes of the non-linear susceptibility $\chi^{(2)}_s$ of Si(100)2×1 were related to the oxygen coverage by a comparison of the results of TPD and SHG experiments. In one series of experiments, the SH signal $[I(2\omega)\propto|\chi^{(2)}_s|^2]$ was recorded before and after the sample was exposed to a desired amount of oxygen. The relative oxygen coverage was then determined from the area of the SiO TPD peaks. Corresponding TPD data are shown in Fig. 1. The adsorption behavior as a function of exposure is plotted in the inset of that figure. It is characterized

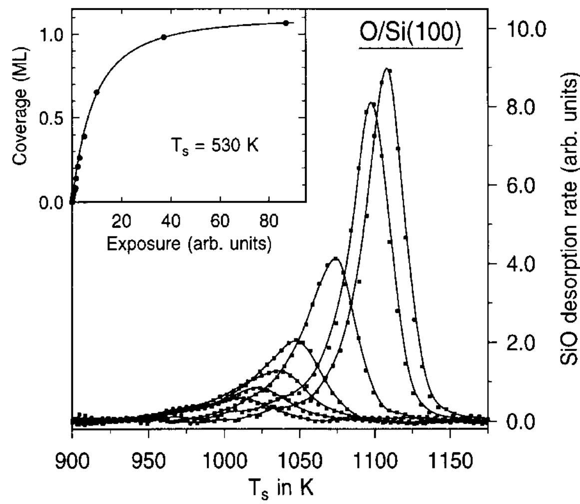

Fig. 1. Thermal desorption traces for SiO from Si(100) for coverages of 0.14, 0.21, 0.26, 0.39, 0.65, 0.98 and 1.07 ML obtained with a linear heating rate of ~14 K s^{-1}. Inset: oxygen coverage of Si(100) versus O_2 exposure at T_s=530 K.

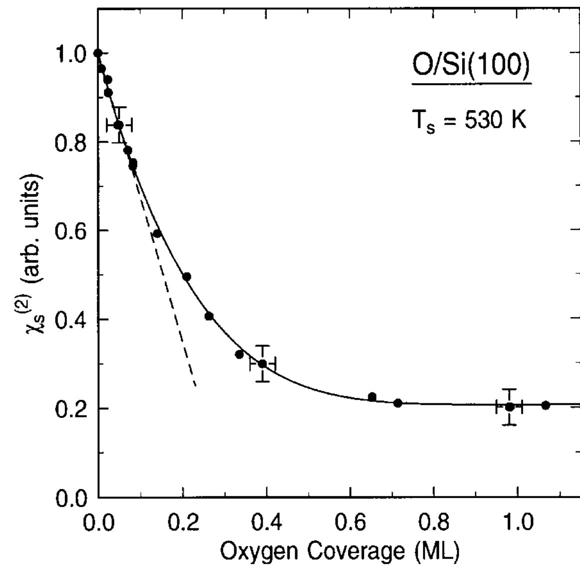

Fig. 2. Decrease of the non-linear susceptibility $\chi^{(2)}_{(s)}$ for Si(100) with oxygen coverage determined from TPD data. The solid line represents the best fit to the data using the model function (Eq. (1)). For coverages $\theta<0.1$ ML, the dependence is approximately linear as indicated by the dashed line.

by a fast initial oxygen uptake followed by a regime of slow oxide growth (not shown). In accordance with the literature [3,15,25], we identify the apparent saturation coverage of the initial oxygen uptake with one monolayer (ML) where 1 ML corresponds to the number of silicon surface atoms [$0.68\times10^{15}\,cm^{-2}$ for Si(100) and $0.78\times10^{15}\,cm^{-2}$ for Si(111)].

The resulting coverage dependence of the absolute magnitude of $\chi^{(2)}_s$ is displayed in Fig. 2. For small oxygen coverages $\theta<0.1$ ML, $\chi^{(2)}_s$ decreases linearly with coverage and then saturates at a value that is five times less than that of the clean surface. With the observed linear relationship, the time dependence $\chi^{(2)}_s(t)$ measured during isothermal desorption experiments at small initial oxygen coverages can be related to $\theta(t)$ without any further considerations.

For oxygen coverages beyond 0.1 ML, it is important to take the detailed functional dependence $\chi^{(2)}_s(\theta)$ into account. A suitable analytical form for $\chi^{(2)}_s(\theta)$ is given by:

$$\chi^{(2)}_s(\theta)=\chi^{(2)}_{s,db}\left(1-\frac{a\theta}{(1+b\theta^{3/2})^3}\right)+\chi^{(2)}_{s,NR}. \quad (1)$$

In this model function, the dominant contribution to the non-linear susceptibility of the clean surface is given by a dangling-bond-derived near-resonant term $\chi^{(2)}_{s,db}$. For small coverages ($\theta\ll b^{-2/3}$), this term decreases linearly with increasing coverages at a slope a. At intermediate coverages, the non-local influence of the adsorbed species on the electronic structure tends to reduce their effect on $\chi^{(2)}$ as their mean separation becomes smaller. We describe this behavior in analogy to the local field corrections to $\chi^{(2)}$ in dense media [26,27]. The coverage-independent non-resonant term $\chi^{(2)}_{s,NR}$ describes the SH response of the saturated surface. Although spectroscopic SH experiments show that the non-linear susceptibility has a coverage-dependent component that is not related to the dangling bonds of the surface [28], the resulting weak coverage dependence of $\chi^{(2)}_{s,NR}$ may be neglected for the purposes of parameterization of $\chi^{(2)}_s(\theta)$.

Since both $\chi^{(2)}_{s,db}$ and $\chi^{(2)}_{s,NR}$ are complex quantities, $\chi^{(2)}_s(\theta)$ is determined by four parameters, the relative magnitude and phase difference of $\chi^{(2)}_{s,db}$ and $\chi^{(2)}_{s,NR}$ and the proportionality constants a and b. The solid line of Fig. 2 shows the result of the best fit of Eq. (1) to the measured data points with

$x^{(2)}_{s,db}/x^{(2)}_{s,NR}=4.9\times\exp(i\times 93.4°)$, $a=3.7$, $b=0.59$. For coverages $h<0.1$ ML, the behavior is, to a good approximation, described by the linear relationship $x^{(s)}(h)\simeq x^{(2)}_{s,0}(1-ah)$ with an average $a\sim 3.0$ similar as in the case of hydrogen adsorption on Si(100) [7].

All SHG experiments described so far have been performed at a temperature of 530 K, and our calibration is strictly valid only at that temperature. At the excitation wavelength of 1064 nm, the ratio $x^{(2)}_{s,db}/x^{(2)}_{s,NR}$ is known to decrease with increasing temperature [29]. In our analysis of the isothermal desorption data, we take this effect into account and adjust the ratio of the SHG signal before and after desorption. Any temperature dependence of a, b, or the phase difference is neglected. Since the desorption rates observed in the experiments described below change by several orders of magnitude, a small uncertainty of our calibration procedure is of negligible influence on the derived kinetic parameter.

In addition to this parameterized analytical calibration curve, a non-analytical functional dependence $x^{(2)}_{s}(h)$ was obtained directly by recording oxygen uptake curves with SHG. An example for O/Si(100) and a surface temperature of 530 K are plotted in the inset of Fig. 3. A calibration curve $x^{(2)}_{s}(h)$ is obtained from the square root of the data and by converting the exposure scale into a coverage scale via the TPD uptake curve (inset of Fig. 1) The TPD-derived coverages are described well by a modified Langmuirian behavior resulting from a sticking probability of the form $s(h)=s_0(1-h/h_{sat})^d$. With $h_{sat}=1.1$ and $d=1.5$, this functional dependence accounts for the fact that after the initial uptake to about 1 ML, the surface is not truly saturated and will continue to adsorb oxygen [15,25].

The resulting calibration curve for Si(100) is plotted in the main panel of Fig. 3. It shows an excellent agreement with the parameterized model function described above. The calibration curve for O/Si(111) was obtained in a similar fashion. We did not perform TPD experiments for this surface. The conversion from the exposure to the coverage scale was rather obtained from a comparison with previous X-ray photoelectron spectroscopy (XPS) experiments [10]. In contrast to

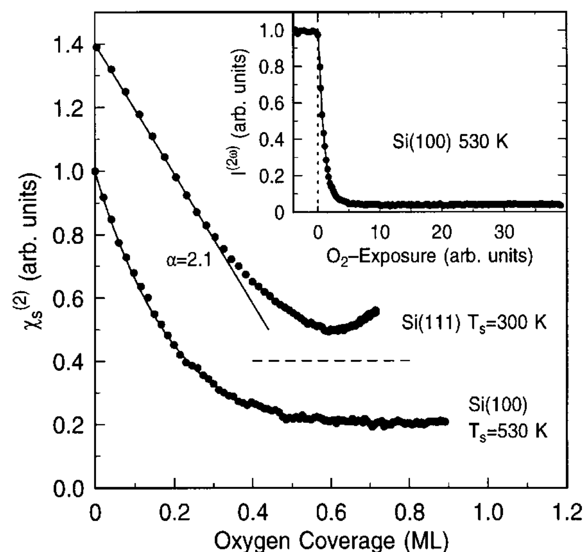

Fig. 3. Non-linear susceptibility $x^{(2)}_{s}$ of Si(111)7×7 and Si(100)2×1 as a function of oxygen coverage. The calibration curve $x^{(2)}_{s}(h)$ is obtained from the square root of the SH intensity and by converting the exposure into a coverage scale using the TPD uptake curve.

Si(100), the Si(111) data exhibit a pronounced minimum of $x^{(2)}_{s}$ at a coverage of ~0.6 ML. According to Eq. (1), this minimum arises from a phase shift of $w>90°$ between the two contributions to $x^{(2)}_{s}$. In the case of hydrogen adsorption on Si(111)7×7, the existence of this phase difference was verified experimentally [7].

From these results, it can be seen that absolute changes in surface coverage of less than 1% of a monolayer can be detected readily with SHG, enabling us to accurately determine desorption rates down to the regime of fractional monolayers of oxygen coverages.

3. Results and discussion

3.1. Si(100)2×1

For the isothermal desorption measurements from Si(100)2×1, the sample is exposed to molecular oxygen at $T_s=530$ K. Then, the sample temperature is increased rapidly to the desired value, and the change in SHG signal is monitored as a

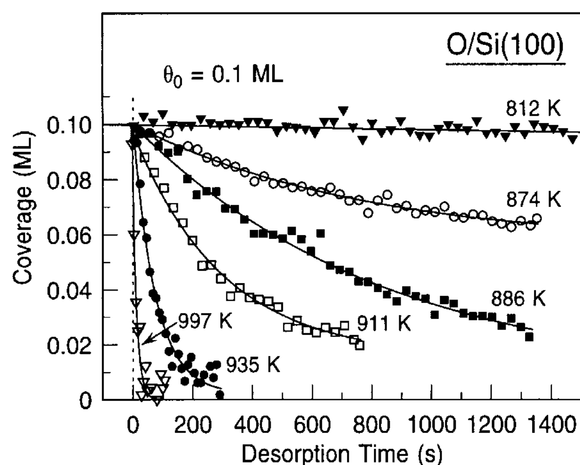

Fig. 4. Isothermal desorption from the Si(100) surface with an initial oxygen coverage of $\theta_0 \simeq 0.1$ ML. The solid curves represent numerical fits assuming an exponential decay of $\theta(t)$.

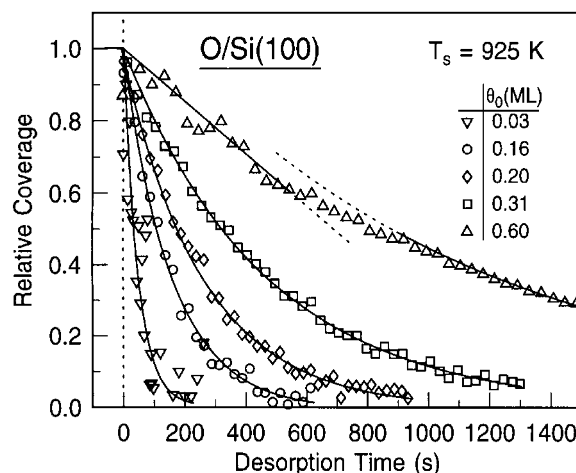

Fig. 5. Isothermal desorption from the Si(100) surface at constant surface temperature of $T_s = 925$ K for different initial coverages θ_0. For a better comparison, the normalized coverages $\theta(t)/\theta_0$ are plotted. The solid curves represent numerical fits, assuming an exponential time dependence, except for $\theta_0 = 0.6$ ML. The line through the initial decay of these data ($t < 600$ s) indicates a constant desorption rate. Desorption at later times ($1000\ \mathrm{s} < t < 3400$ s) is again compatible with $\theta(t) \propto \exp(-\nu_d t)$.

function of time. After complete desorption of the oxide, the non-linear susceptibility approaches its initial value measured for the clean surface for that particular temperature. After each desorption experiment, the sample is annealed at 1300 K and cooled at a rate of 1–2 K s^{-1} in order to prepare a well-ordered substrate for the subsequent measurement.

Fig. 4 shows the resulting time dependence of the surface coverage for a number of different temperatures starting with the same initial coverage of $\theta_0 \simeq 0.1$ ML. Data corresponding to different initial coverages but fixed desorption temperatures are collected in Fig. 5. For the purpose of data analysis, we assume first-order kinetics for the desorption process:

$$R_d = -\frac{d\theta}{dt} = \theta(t)\nu_d(\theta, T_s) = \theta(t)\nu_0(\theta)\exp\left(-\frac{E_A(\theta)}{k_B T_s}\right) \qquad (2)$$

with a coverage- and temperature-dependent rate constant $\nu_d(\theta, T_s)$. Its (exponential) temperature dependence is expressed in terms of an activation energy $E_A(\theta)$ and a pre-exponential factor $\nu_0(\theta)$ in the usual way.

The signal-to-noise ratio of the individual desorption traces does not allow for an independent, accurate determination of the coverage and temperature dependence of $\nu_d(\theta, T_s)$. In order to deduce activation energy and prefactor, we compare data with the same initial coverage θ_0 (Fig. 4), neglect the coverage dependence [$\nu_d(\theta) = \mathrm{const.}$] and determine the rate constant from numerical fits to the resulting simple exponential time evolution $\theta(t) = \theta_0 \exp(-\nu_d t)$. The resulting Arrhenius plot is discussed in Section 3.3 (Fig. 8). The coverage dependence of the rate constants is determined from sets of data with varying initial coverages taken at fixed desorption temperatures. The rate constants deduced from the data displayed in Fig. 5, from other data at $T_s = 925$ K, and from a set of data obtained at a desorption temperature of $T_s = 876$ K are collected in Fig. 6.

In Fig. 6, the rate constants $\nu_d = R_d/\theta$ are plotted as a function of the inverse coverage $1/\theta_0$. In this representation, they would be constants for a strict first-order desorption process ($-d\theta/dt \propto \theta$), but would increase linearly for zero-order kinetics ($d\theta/dt = \mathrm{const}$). For coverages $\theta_0 > 0.1$ ML, the

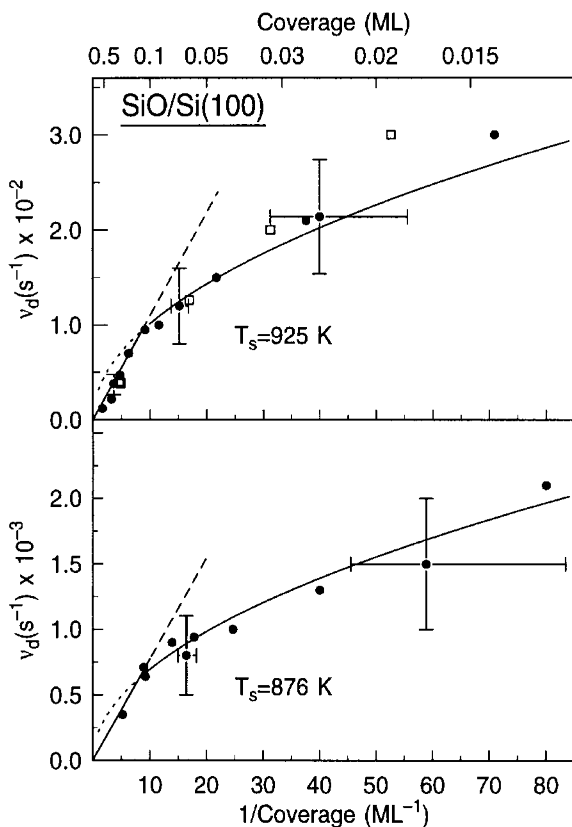

Fig. 6. Desorption rate constants $n_d = R_d/h$ for isothermal desorption experiments from the Si(100) surface as a function of the inverse initial oxygen coverage $1/h_0$. The straight and curved solid lines indicate the behavior expected for apparent kinetic orders of 0 and 1/2, respectively. The square symbols at coverages of 0.02, 0.03 and 0.06 ML represent data obtained without annealing the surface after the desorption of 0.2 ML oxygen.

rate constants appear to be consistent with the latter behavior. For $h_0 \leq 0.1$ ML, the coverage dependence is intermediate and can be described by an apparent kinetic order of one half ($-dh/dt \propto h1/2$). Such behavior is typical for desorption from the boundaries of two-dimensional islands [30]. While their mean area is proportional to the coverage, the number of atoms at the boundaries scale like h1/2. It is noted that for $h_0 < 0.3$ ML also the individual desorption measurements are found to be compatible with the corresponding temporal dependence $h(t) = h_0(1 - at)2$. For higher coverages, the desorption traces can be described neither by simple first- nor by half-order kinetics. In the case of the highest initial coverage used in the present investigation ($h_0 = 0.6$ ML), the desorption starts with an almost coverage-independent rate. This behavior is in qualitative agreement with earlier isothermal desorption measurements by means of XPS, which showed a transition from apparent zero-order to first-order kinetics for coverages between 0.7 and 1 ML [15].

From STM studies, it is known that during the desorption, the surface undergoes substantial roughening [31]. In order to address the question as to the extent to which surface roughening during the desorption process influences the desorption kinetics, the following experiments were performed: 0.2 ML oxygen is adsorbed on the well prepared surface and then desorbed isothermally at $T_s = 925$ K. In a subsequent experiment, 0.03 ML is adsorbed at 530 K without prior annealing of the surface. The desorption trace of the so prepared oxide layer is shown as a dashed line in Fig. 5. The same experiments were repeated with the same pre-dose coverage but different subse-

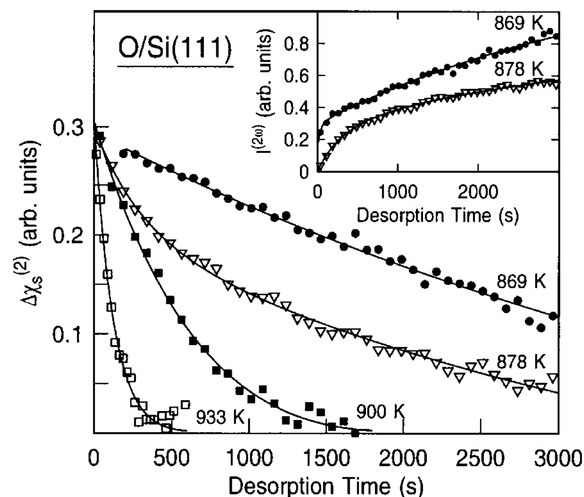

Fig. 7. Relative change of the nonlinear susceptibility of Si(111) during isothermal desorption of 0.3 ML oxygen at various temperatures. The inset shows two representative SH-intensity traces as a function of time measured at different surface temperatures. The initial fast signal increase is associated with rearrangement processes, whereas the subsequent slower change is related to desorption.

quent coverages of 0.02 and 0.06 ML. The resulting desorption rate constants are shown in Fig. 6 as open squares. Obviously, there are no observable differences in the desorption behavior from the initially well-prepared surface compared with the slightly roughened surface.

3.2. *Si(111) 7×7*

SiO desorption from Si(111) was investigated for an initial coverage of 0.3 ML. The measured SH response during isothermal desorption is displayed in Fig. 7 for four different surface temperatures. It exhibits a more complex time dependence as compared with the Si(100) surface, in particular for temperatures below 900 K. In this regime, the decay of $\Delta\chi_s^{(2)}(\theta) \equiv \chi_{s(0)}^{(2)} - \chi_s^{(2)}(\theta)$ is characterized by two time constants. This behavior is clearly visible already in some of the raw data (Fig. 7, inset). For the purposes of analysis, we describe the decay of $\Delta\chi_s^{(2)}$ by two exponentials and identify the slow time constant with the desorption rate of SiO. Between 800 and 880 K, the rates associated with the fast process vary from $10^{-3}\,s^{-1}$ to $5\times10^{-2}\,s^{-1}$, whereas in the same temperature range, the desorption rates lie between 10^{-6} and $3\times10^{-4}\,s^{-1}$. Both rates are thus sufficiently distinct and allow for an independent determination. For temperatures above 900 K, $\Delta\chi_s^{(2)}$ is well described by a single exponential decay.

The fast initial increase of the SH signal is likely to be caused by a rearrangement process of the adsorbate layer prior to desorption, which leads to an increased number of dangling bonds. This interpretation is suggested by previous XPS results. After oxygen exposure at room temperature, the Si 2p core levels show satellites that are commonly interpreted in terms of silicon oxidation stages ($Si1^+$ to $Si4^+$) [32,33]. After annealing at 750 K, the intensity of the $Si3^+$ and $Si4^+$ is observed to increase at the expense of $Si1^+$ and $Si2^+$ [32]. STM investigations have related this behavior to oxygen island formation on the surface [34].

Oxygen adsorption on Si(111) 7×7 is preceded by a metastable molecular precursor [6,35,36]. An interesting question that arises from recent work concerning this system is whether the rearrangement process is in fact caused by diffusion of molecular rather than atomic oxygen. Using a variable-temperature STM, Tsong et al. [37] recently observed diffusive motion of so-called ''bright'' oxygen-induced sites on Si(111) 7×7 and suggested that this is caused by the diffusion of the O_2 precursor. Also, the fact that we observe the kind of arrangement process only for the Si(111) and not for the Si(100) surface would be consistent with O_2 diffusion driving the clustering of oxygen on the surface. However, it seems unlikely that molecular oxygen is able to persist at temperatures as high as 900 K. We consistently find that molecular oxygen dissociates quickly at surface temperatures above 500 K [10,38]. Similar findings have been reported by others [39,40]. As neither the STM nor SHG is able to distinguish unambiguously between molecular and dissociated oxygen species, further experiments will be necessary in order to give a definite answer to the origin of the rearrangement process.

3.3. *Arrhenius parameters*

The desorption rates obtained for Si(100) with initial oxygen coverage of $\theta_0 \simeq 0.1$ ML are displayed in Fig. 8 in the form of an Arrhenius plot. As a result of the high adsorbate sensitivity of SHG, the desorption can already be monitored for temperatures as low as 780 K. From the figure, it can be seen that isothermal desorption measurements allow the evaluation of desorption rate constants over five orders of magnitude ranging from $10^{-6}\,s^{-1}$ to $10^{-1}\,s^{-1}$. Higher values can hardly be obtained using the isothermal desorption technique because of the finite heating rate that has to be applied to reach the desired temperature. The background pressure in the chamber determines the low temperature limit for acquiring desorption rates.

The activation energy deduced for Si(100) is $E_A = 3.4 \pm 0.2$ eV with a prefactor $\nu_0 = 10^{16\pm1}\,s^{-1}$. The error of these values is dominated by the accuracy of the temperature measurement. For comparison, results from a modulated molecular beam reactive scattering (MMBRS) experiment [15] are included in the figure. Our data extend the range of rate constants obtained so far with

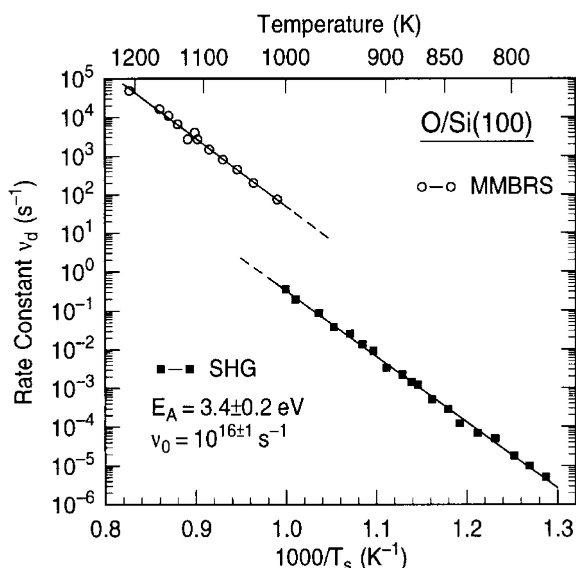

Fig. 8. Arrhenius plot of the measured first-order rate constant n_d for SiO desorption from Si(100) for an initial oxygen coverage h_0 = 0.1 ML (filled squares). The data marked with open circles represent results obtained from molecular beam scattering experiments [15].

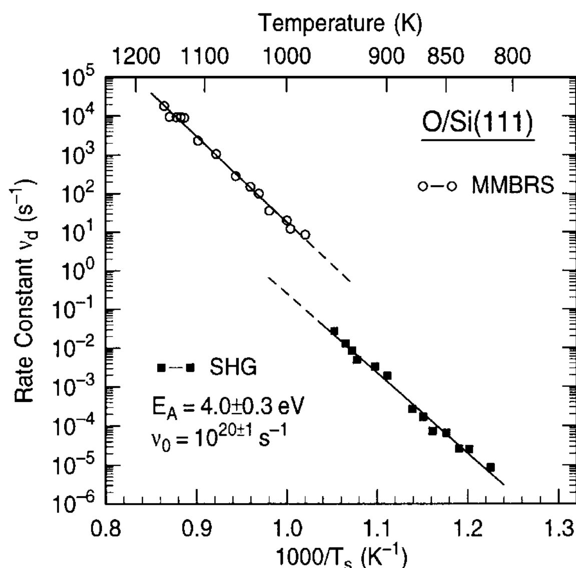

Fig. 9. Arrhenius plot of the measured desorption rate constants for Si(111) for an initial oxygen coverage of 0.3 ML. The open circles represent results obtained from molecular beam scattering experiments [19].

MMBRS and TPD [22] by more than four orders of magnitude towards lower temperatures.

The desorption rates for the (111) oriented surface are shown in Fig. 9. These values lead to an activation energy of $E_A = 4.0 \pm 0.3$ eV with pre-exponential $n_0 = 10^{20\pm1}$ s^{-1}. The MMBRS experiment shown for comparison [19] results in an activation energy of 4.4 ± 0.2 eV, which is in good agreement with our value.

Between 780 and 1200 K, the rates for SiO desorption vary over nearly 11 orders of magnitude. Strikingly, over the whole range, the desorption reaction obeys the Arrhenius law. The activation energies, E_A, obtained using the different techniques of SHG, TPD and MMBRS are found to be in fairly good agreement with each other and seem to vary only slightly with initial coverage. For Si(100), the TPD values concentrate in the range of 3.5–3.9 eV [21,22], from MMBRS values of 4.0 ± 0.4 [19], 3.5 ± 0.1 [15], 3.4 ± 0.1 [18] and 3.0 eV [16] are reported. Values of 2.8 ± 0.05 eV were reported from Ohkubo et al. [20] for both Si(100) and Si(111) using the scattering technique. This energy appears to be too small compared with our values and those from other studies. In a recent investigation, TPD was used to study SiO desorption from Si(100) after dissociative adsorption of water [41]. The obtained activation energies of 3.3 and 3.5 eV for initial D_2O coverages of 0.05 and 0.4 ML, respectively, are in excellent agreement with the 3.4 eV from our experiment for 0.1 ML.

Although the activation energies are quite similar, the pre-exponential factors n_0 deduced from the scattering experiments are two to four orders of magnitude larger than those obtained by TPD and SHG. This is likely a consequence of the different oxygen coverages in these experiments. Whereas most of the TPD studies were carried out from oxidized surfaces with high oxygen coverages (>0.1 ML), the coverages in the MMBRS experiments are typically 10^{-3} ML and below [3]. Quantitatively, the prefactors reported in the literature vary between 10^{16} [16,20] and 10^{20} s^{-1} [15]. Our value of 10^{16} s^{-1} for the Si(100) surface obtained for an initial oxygen coverage of 0.1 ML again agrees well with that from the TPD study [41], which reported a range between 2.5×10^{17}

and $2.5\times10^{16}\,s^{-1}$ for D_2O coverages of 0.05–0.4 ML.

Unanimously, the observed pre-exponentials are remarkably large and exceed the values for most other adsorbate systems by two or more orders of magnitude. Within the framework of transition state theory (TST), a high-frequency factor n_0 would require desorption to occur via the excitation of a strongly localized initial state into a highly mobile transition state. The upper limit for n_0 is then described by the ratios of the total partition functions of the activated complex and the adsorbed particle, whereas the rotational and translational degrees of freedom contribute most strongly [42]. Assuming that the activated complex can be represented solely by a rotating SiO, n_0 would already be of the order of $10^{16}\,s^{-1}$ calculated for a temperature of 800 K. If, in addition, two-dimensional motion or another rotational contribution is taken into account, n_0 can easily reach values of $10^{19}\,s^{-1}$. Alternatively, using three bending modes in addition to one free internal rotation of the SiO, the frequency factor can be calculated to be of the order of $10^{17}\,s^{-1}$.

3.4. Discussion of the desorption mechanism

The similar kinetic parameter describing the desorption from Si(100) and Si(111) indicates that microscopic details due to the different surface orientations apparently do not strongly affect the desorption process. Recently, the dynamics of the SiO desorption has been addressed by REMPI spectroscopy in reactive oxygen scattering experiments [43,44]. A very similar behavior of Si(100) and Si(111) was also observed in these studies. The vibrational and rotational energies of the desorbing SiO molecules were found to be in thermal equilibrium with the silicon surface, indicating that the desorption follows a reaction path going through a state in which SiO is almost freely rotating [44]. The results thus support the estimate of the prefactor given above. Furthermore, from the validity of the Arrhenius law over nearly 11 orders of magnitude, it may be concluded that there is a common underlying microscopic mechanism in the desorption process, regardless of whether the reaction occurs upon the interaction of individual oxygen atoms with the bare surface at a high temperature or at finite coverages and a temperature below the critical temperature for surface etching.

For a further discussion of the microscopic reaction steps involved in SiO desorption, it is important to recall the information that has been obtained from spatially resolved investigations [31,45–47]. The thermal decomposition of thick (50–500 Å) as well as that of ultrathin oxide films proceeds inhomogeneously from the perimeters of circular voids or shrinking oxide islands without thinning of the remaining oxide and voids exposing the bare silicon substrate [45–47]. Even for monolayer desorption from Si(100), the formation of growing voids could be clearly observed by Johnson and Engel with the STM [31]. Because the growth rate of the voids was found to scale with their area, these authors suggested that the formation of mobile silicon monomers inside the void area is the rate-limiting step of the desorption process. The monomers were suggested to diffuse to the void perimeter, react with oxygen and form volatile SiO [31].

Such a mechanism, however, is very unlikely to be operative at small oxygen coverages. It would lead to apparent zero-order kinetics [$R_d \propto (1-h) \approx$ const. for $h \to 0$], which we can clearly exclude for $h < 0.3$ ML. Furthermore, one would expect an enhanced desorption rate when oxygen is desorbed from a pre-roughened surface, where monomers should form more readily. Also, such a behavior is in contrast to the results described in Section 3.1. Previous beam experiments actually showed that the rate even decreases somewhat with increasing etch of the surface [15]. Finally, the creation of Si monomers at the steps and likewise also at defects of a rough surface is likely to require considerably less activation energy [48,49] than the 3.4 eV measured for SiO desorption. If the creation of diffusing monomers would really be the rate-limiting step for volatile SiO production on the surface, one would expect desorption to take place already at temperatures as low as 600 K when step flow on Si(100) becomes significant, in striking contrast to the available experimental information.

We think that the actual oxygen binding config-

uration is the key to understand the highly complex desorption behavior of SiO. As a result of the insertion reaction of oxygen between two silicon atoms [32,35,50], the average coordination number equivalent to the oxidation stages of the silicon atoms increases with increasing coverage, as discussed in Section 3.2. This has a stabilizing effect on the oxide layer and therefore results in a reduced desorption rate of aggregated as compared with isolated oxygen species. Following up the ideas of D'Evelyn et al. [15], we suggest that the desorption at finite coverages occurs at the boundaries of oxygen islands and is preceded by the formation of the least coordinated isolated Si–O–Si species with a formal oxidation state of 1+. Fission of Si–O and Si–Si bonds leads to the activated SiO (a) state and desorption of gas phase SiO (g):

$$Si(2^+,3^+,4^+)O \rightleftharpoons Si1^+O \rightleftharpoons SiO(a) \rightarrow SiO(g). \quad (3)$$

The overall activation barrier for desorption is clearly dominated by the reaction enthalpy of the last process. Otherwise, we would expect the activation energy determined by MMBRS where only isolated oxygen species are involved in the reaction to be much lower than the values determined by SHG or TPD. However, the error bars of ± 0.2–0.3 eV of our activation energies are still compatible with an energy difference between high and low coordinated species that is sufficient to prevent small oxygen islands to dissolve at low coverages. Furthermore, oxygen clusters conceivably become stabilized kinetically with increasing size.

Within the framework of this model, the coverage dependence of the desorption rate can be explained in a straightforward way. Even at low coverages of a few per cent of a monolayer, oxygen forms two-dimensional islands with an average circumference that is proportional to the square root of the coverage leading to apparent half-order desorption kinetics. When the coverage increases to half a monolayer and beyond, the oxygen coordination of silicon increases within the islands as seen in an increase of the relative amount of the most stable $Si4^+O$ in XPS [32]. The desorption rate from the boundaries of these thicker islands becomes even less dependent on the total oxygen coverage. Since oxygen islands are not formed under the conditions of the beam experiments, the rate constants are appreciably higher in this case.

An alternative explanation for the STM results of Johnson and Engel is possible under the assumption that the layers are not in thermal equilibrium before desorption. In this case, there will not only be desorption during the time the sample is heated. Oxygen rearrangement and aggregation within the oxidized area is likely to occur simultaneously. This might contribute to the faster void growth reported in Ref. [31]. The fact that diffusional equilibrium is not readily achieved under the conditions of typical desorption experiments was actually demonstrated with TPD studies using isotopically labeled oxygen [2]. The results by Shklyaev et al. [13] mentioned in the introduction corroborate such an interpretation. Their SHG experiments, performed at the Si(111) surface in the temperature regime between 880 and 1070 K clearly showed that slowly grown oxides are more stable towards decomposition than less equilibrated oxygen layers formed rapidly under conditions of high oxygen pressures.

4. Conclusion

The isothermal desorption of SiO from Si(100) and Si(111) has been studied by SHG for a wide range of temperatures and initial coverages. The rates obey an Arrhenius law and activation energies of $E_A = 3.4 \pm 0.2$ and 4.0 ± 0.3 eV were obtained for Si(100) and Si(111), respectively. Whereas the activation energy exhibits little or no dependence on the initial oxygen coverage, the first-order rate constants are found to increase by more than an order of magnitude when the initial oxygen coverage is decreased from 0.6 to 0.02 ML. The observed behavior is compatible with a model where isolated SiO units are formed at the boundaries of oxygen islands. With this study, we demonstrate the applicability of surface SHG to obtain quantitative results for complex chemisorbates, opening real-time insight into desorption and related processes not easily accessible with other techniques. In order to reach a more definite conclusion about the detailed microscopic mecha-

nisms, experiments that address both the kinetic and structural aspects of the desorption process, e.g. by combining SHG with an atomic scale imaging technique such as STM, would be highly desirable.

Acknowledgements

The authors would like to thank K.L. Kompa for continuous support and acknowledge funding by the Deutsche Forschungsgemeinschaft through Sonderforschungsbereich 338.

References

[1] N.F. Mott, S. Rigo, F. Rochet, A.F. Stoneham, Philos. Mag. B 60 (1989) 189.
[2] H.C. Lu, E.P. Gusev, E. Garfunkel, T. Gustafsson, Surf. Sci. 351 (1996) 111.
[3] Th. Engel, Surf. Sci. Rep. 18 (1993) 91.
[4] A. Feltz, U. Memmert, R.J. Behm, Surf. Sci. 314 (1994) 34.
[5] J.V. Seiple, J.P. Pelz, Phys. Rev. Lett. 73 (1994) 999.
[6] R. Martel, Ph. Avouris, I.-W. Lyo, Science 272 (1996) 385.
[7] U. Höfer, Appl. Phys. A 63 (1996) 533.
[8] T.F. Heinz, M.M.T. Loy, W.A. Thompson, J. Vac. Sci. Technol. B 3 (1995) 1467.
[9] H.W.K. Tom, X.D. Zhu, Y.R. Shen, G.A. Somorjai, Surf. Sci. 167 (1986) 167.
[10] P. Bratu, U. Höfer, Phys. Rev. Lett. 74 (1995) 1625.
[11] A.A. Shklyaev, T. Suzuki, Phys. Rev. Lett. 75 (1995) 272.
[12] A.A. Shklyaev, M. Aono, T. Suzuki, Phys. Rev. B 54 (1996) 10890.
[13] A.A. Shklyaev, T. Suzuki, Surf. Sci. 351 (1996) 64.
[14] K. Nakamura, A. Kurokawa, S. Ichimura, J. Vac. Sci. Technol. A 15 (1997) 2441.
[15] M.P. D'Evelyn, M.M. Nelson, Th. Engel, Surf. Sci. 186 (1987) 75.
[16] M.L. Yu, B.N. Eldridge, Phys. Rev. Lett. 58 (1987) 1691.
[17] J.R. Engstrom, T. Engel, Phys. Rev. B 41 (1990) 1038.
[18] J.R. Engstrom, D.J. Bonser, M.M. Nelson, T. Engel, Surf. Sci. 256 (1991) 317.
[19] U. Memmert, M.L. Yu, Surf. Sci. 245 (1991) L185.
[20] K. Ohkubo, Y. Igari, S. Tomoda, I. Kusunoki, Surf. Sci. 260 (1992) 44.
[21] Y.-K. Sun, D.J. Bonser, Th. Engel, Phys. Rev. B 43 (1991) 14309.
[22] Y.-K. Sun, D.J. Bonser, Th. Engel, J. Vac. Sci. Technol. A 10 (1992) 2314.
[23] P. Feulner, D. Menzel, J. Vac. Sci. Technol. 17 (1980) 662.
[24] T.F. Heinz, in: H.-E. Ponath, G.I. Stegeman (Eds.), Nonlinear Surface Electromagnetic Phenomena, North-Holland, Amsterdam, 1991, p. 353.
[25] W. Ranke, D. Schmeisser, Surf. Sci. 149 (1985) 485.
[26] Y.R. Shen, The Principles of Nonlinear Optics, Wiley, New York, 1984.
[27] M. Kuchler, F. Rebentrost, Phys. Rev. B 50 (1994) 5651.
[28] W. Daum, H.-J. Krause, U. Reichel, H. Ibach, Phys. Rev. Lett. 71 (1993) 1234.
[29] U. Höfer, Leping Li Li, G.A. Ratzlaff, T.F. Heinz, Phys. Rev. B 52 (1995) 5264.
[30] J.R. Arthur, A.Y. Cho, Surf. Sci. 36 (1973) 641.
[31] K.E. Johnson, T. Engel, Phys. Rev. Lett. 69 (1992) 339.
[32] G. Hollinger, J.F. Morar, F.J. Himpsel, G. Hughes, J.J. Jordan, Surf. Sci. 168 (1986) 609.
[33] P. Morgen, U. Höfer, W. Wurth, E. Umbach, Phys. Rev. B 39 (1989) 3720.
[34] Y. Ono, M. Tabe, H. Kageshima, Phys. Rev. B 48 (1993) 14291.
[35] U. Höfer, P. Morgen, W. Wurth, E. Umbach, Phys. Rev. Lett. 55 (1985) 2979.
[36] G. Dujardin et al., Phys. Rev. Lett. 73 (1994) 1727.
[37] I.-S. Hwang, R.-L. Lo, T.T. Tsong, Phys. Rev. Lett. 78 (1997) 4797.
[38] U. Höfer, P. Morgen, W. Wurth, E. Umbach, Phys. Rev. B 40 (1989) 1130.
[39] Ph. Avouris, I.-W. Loy, F. Bozso, J. Vac. Sci. Technol. B 9 (1991) 424.
[40] C. Silvestre, M. Shayegan, Phys. Rev. B 37 (1988) 10432.
[41] M.C. Flowers, N.B.H. Jonathan, A. Morris, S. Wright, Surf. Sci. 352 (1996) 87.
[42] V.P. Zhdanov, Surf. Sci. Rep. 12 (1991) 183.
[43] K.G. Nakamura, M. Kitajima, J. Chem. Phys. 102 (1995) 8569.
[44] K.G. Nakamura, I. Kamioka, M. Kitajima, J. Chem. Phys. 104 (1996) 3403.
[45] M. Liehr, J.E. Lewis, G.W. Rubloff, J. Vac. Sci. Technol. A 5 (1987) 1559.
[46] G.W. Rubloff, J. Vac. Sci. Technol. A 8 (1990) 1857.
[47] Y. Kobayashi, K. Sugii, J. Vac. Sci. Technol. A 10 (1992) 2308.
[48] B.S. Swarzentruber, M. Schacht, Surf. Sci. 322 (1995) 83.
[49] Ch. Pearson, B. Borovsky, M. Krueger, R. Curtis, E. Ganz, Phys. Rev. Lett. 74 (1995) 2710.
[50] H. Ibach, H.D. Bruchmann, H. Wagner, Appl. Phys. A 29 (1982) 113.